Studying Transient Carrier Behaviors in Pentacene Field Effect Transistors Using Visualized Electric Field Migration

ARTICLE *in* THE JOURNAL OF PHYSICAL CHEMISTRY C · JUNE 2009

Impact Factor: 4.77 · DOI: 10.1021/jp900779d

4 AUTHORS, INCLUDING:

Fei Liu
Wuxi University of Light Industry
350 PUBLICATIONS **3,501** CITATIONS

SEE PROFILE

Martin Weis
Slovak University of Technology in Bratislava
143 PUBLICATIONS **840** CITATIONS

SEE PROFILE

M. Iwamoto
Tokyo Institute of Technology
117 PUBLICATIONS **1,361** CITATIONS

SEE PROFILE

Studying Transient Carrier Behaviors in Pentacene Field Effect Transistors Using Visualized Electric Field Migration

Takaaki Manaka,*,† Fei Liu,‡ Martin Weis,† and Mitsumasa Iwamoto*,†

Department of Physical Electronics, Tokyo Institute of Technology, 2-12-1 O-okayama, Meguro-ku, Tokyo 152-8552, Japan, and Center for Advanced Study, Tsinghua University, Beijing 100084, China

Received: January 27, 2009; Revised Manuscript Received: March 25, 2009

Time-resolved microscopic optical second harmonic generation (TRM-SHG) imaging was used to study the transient carrier behaviors in pentacene field effect transistor (FET) with Au and Ag electrodes on the basis of the migration of the electric field profile. We found that the time evolution of the electric field distribution in the pentacene FET channel was quite different between the devices using Ag and Au electrodes: enhanced SHG signal representing insufficient carrier accumulation decayed rapidly at the edge of the Au source electrode, while the signal decayed but remained at the edge of the Ag electrode. Interestingly, the peaks of the SHG signal depicting the edge of the carrier sheet in the channel region in both cases migrated in a way of the square root of time. A simple model was proposed to uniformly account for the experimental observations, and a numerical simulation on the transient carrier behaviors with the electric field migration using two-dimensional coupled diffusion-drift and the Poisson equations well-supported this model. Particularly, the results showed that the evaluated carrier mobility in the FET channel based on this model was independent of the metal electrode, indicating identical carrier transport in the bulk between the devices using Au and Ag electrodes.

I. Introduction

Metal−semiconductor contact plays an important role in electronic devices. In particular, the electrical characteristics of organic electronic devices depend strongly on the organic−metal contact because injected carriers dominate the device operation. For instance, ambipolar behavior in organic field effect transistors (OFETs) was observed using appropriate electrode metals; i.e. electrons and holes were selectively injected from small and large work function electrodes, respectively.[1−3] For the silicon (Si) and other inorganic semiconductors, the type of semiconductor, i.e., n- or p-type, is determined by a doping condition, and the metal−semiconductor contact is well-defined energetically on the basis of the thermodynamic equilibrium theory of the Fermi−Dirac statistics.[4] The situation is more complicated and the knowledge of contact becomes more helpful for operating organic devices efficiently, because fabrication processes such as deposition of an organic layer and the metal electrode significantly affect device performance.[5,6] There are many ambiguities in interfacial energetics at the organic−metal contact due to the presence of dipoles and interaction between molecules and electrode, etc.[7] The adequate control of injection and transport processes is still not satisfactory. Hence, to disclose the charge-transport mechanism and to improve organic device capability, individual evaluation of the injection and transport processes is important.

Nevertheless, from a single current−voltage measurement, injection and transport processes could not be evaluated independently, because channel resistance and contact resistance are connected in series in the equivalent circuit of OFET. Consequently, a field effect mobility that is evaluated from $I_{ds} - V_{gs}$ characteristics depends on the electrode metals. For p-channel operation, large mobility was reported using high work function electrodes,[8,9] suggesting that there is an intimate relationship between the work function of the injection electrode and the mobility. Essentially, however, mobility should be an intrinsic parameter that depends on the organic semiconductor materials. Such a contradictory discussion step from the conventional $I-V$ measurements can be resolved by employing the independent evaluation of the injection and transport processes. Further, difference in the electrode metals becomes more critical for the bottom contact FET, because the organic active materials are deposited on metal surfaces. For the vacuum evaporation of organic materials, the crystalline structure depends strongly on metals.[10] In such a case, both injection and transport processes are affected by the metal electrode. To discuss the device operation of OFET, a complex change in the carrier processes should be discriminated in detail.

Many optical techniques have been proposed for investigating the organic devices, such as Raman spectroscopy,[11] infrared (IR) spectroscopy,[12] and sum frequency generation (SFG).[13] These enable us to study the interaction between molecules and carriers as a molecular vibration. Hence, these researches have mainly focused on energetics of carriers, and have not yet paid attention to the above-mentioned fundamental issues, i.e., individual evaluation of the injection and transport processes. On the other hand, we have developed a time-resolved microscopic SHG (TRM-SHG) measurement for visualizing carrier motion in the organic thin film transistors[14] on the basis of electric field induced optical second harmonic generation (EFISHG). Carrier motion can be observed by following the time evolution of the electric field distribution in the devices. Direct observation of the electric field is one of the prominent advantages of the EFISHG, because carrier injection and transport processes are clearly visualized in time, and this fact allows us to evaluate these two processes individually. Knowing the information about

* E-mail: manaka@ome.pe.titech.ac.jp (T.M.); iwamoto@pe.titech.ac.jp (M.I.).
† Tokyo Institute of Technology.
‡ Tsinghua University.

10.1021/jp900779d CCC: $40.75
Published on Web 05/18/2009

the electric field within the devices in transient and steady states obtained using TRM-SHG measurement gives an individual understanding of the injection and succeeding transport mechanisms of the carrier. In our previous work, we revealed a diffusion-like behavior of the electric field migration along pentacene FET using the TRM-SHG measurement.[15] In this work, we further used the TRM-SHG method to investigate carrier behaviors in pentacene FET, i.e., the transport and injection of carriers, from a viewpoint of the electric field migration with different metal electrodes. We found that the migration behavior of the electric field in the FET channel was significantly distinct for different metals. On the basis of a numerical simulation, we suggested that the difference arose from the distinct carrier injection capacity of the metals, which was determined by the work function of the metals. Moreover, we introduced a simple model describing the carrier motion in the channel region. This model made the evaluation of the mobility by TRM-SHG method possible, and we could show that although the carrier behavior was dependent on the work function of the metals, the evaluated carrier mobility in the channel region had no dependence on the work function of metals.

II. Experiments

Samples used in the experiments were top-contact FET structures. Heavily doped Si wafers covered with a 500 nm thick oxide (SiO_2) layer were used as the base substrate. The material for the organic semiconductor layer was pentacene ($C_{22}H_{14}$). Before the pentacene deposition, a 100 nm thick poly(methyl methacrylate) (PMMA) layer was spin-coated in order to improve the on−off ratio of the devices. Then, the pentacene layer, approximately 100 nm thick, was deposited on a surface. The process pressure during the deposition of pentacene was kept at less than 1×10^{-4} Pa, and the deposition rate was controlled at approximately 3 nm/min. After the deposition of pentacene, top-Au or -Ag electrodes (source and drain electrodes) with a thickness of 100 nm were deposited. The designed channel length (L) and width (W) were 30 μm and 3 mm, respectively. Pentacene FETs were operated with the application of pulse voltages using a function generator (NF Corp., WF1947) and a high-speed bipolar amplifier (NF Corp., HSA4101). All measurements were performed in laboratory ambient atmosphere.

The light source for the TRM-SHG measurement was an optical parametric oscillator (OPO; Continuum Surelite OPO) pumped by the third-harmonic light of a Q-switched Nd:YAG laser (Continuum, SureliteII-10). The external Q-switch signal of a YAG laser was also supplied from a function generator to synchronize between the voltage pulse applied to OFET and the laser pulse. The timing chart of the voltage pulse applied to OFET and the laser pulse was represented in ref 7. Fundamental light was focused onto the channel region of OFET with normal incidence using a long working distance objective lens (Mitutoyo, M Plan Apo SL20×; NA = 0.28; working distance WD = 30.5 mm). The fundamental light almost uniformly irradiated across the channel for taking the SHG image by using a beam expander (see Figure 1a). Spatial and temporal resolution were 0.5 μm and 20 ns, respectively. Selecting an appropriate wavelength is important to observe the SHG signal from pentacene effectively, because the SHG intensity strongly depends on the fundamental wavelength. The fundamental wavelength was fixed at 1120 nm in this study. SH light generated from the FET was filtered by a fundamental-cut filter and an interference filter to remove fundamental and other unnecessary light. Finally, the SH light generated was detected by a cooled CCD camera (Andor Technology, DU420-BV). In this configuration, the polarization direction of the fundamental light was chosen in the direction corresponding to the channel direction (the source-drain direction).

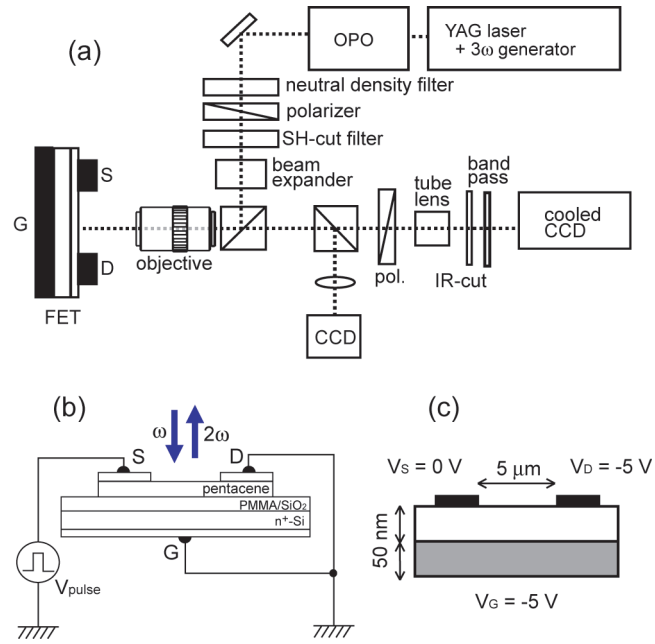

Figure 1. (a) Optical setup for the SHG imaging. S, D, and G in the FET represent respectively the source, drain, and gate electrodes. (b) Schematic images of the sample structure of the pentacene FET and electrical connection. Note the drain and gate electrodes were electrically shorted and connected to ground. (c) Device structure and the parameters for numerical simulation. The thicknesses of the gate insulator and pentacene film are the same.

III. Results

Figure 2 shows the change in the SHG intensity distribution along the FET channel with different delay times (time between the laser pulse and the rising edge of the positive voltage pulse). An actual SHG image from the OFET channel is shown in the inset of Figure 2b as an example. The SHG intensity distribution was obtained from the SHG image by taking a line scan of the SHG image. Parts a and b of Figure 2 represent the cases of positive pulse application to the Au and Ag source electrodes, respectively, where the applied voltage was 100 V, and the source electrode is defined as an electrode from which carriers are injected by the applied voltage pulse (see also Figure 1b). As shown in the figure, the SHG peak moved rapidly from the source to the drain electrode with an increase of the delay time, indicating that the injected holes from the source electrode spread immediately in the FET channel.

As discussed in our previous paper,[15] the motion of the SHG peak in the case of the Au electrode followed a diffusion-like behavior, namely, the square of the SHG peak position was proportional to time (see Figure 3a). For the devices using Ag electrode, the SHG peak also moved from the source to the drain electrode, though it seemed to be slow compared with the Au case. As shown in Figure 3b, an evaluated slope in log−log scale time evolution for the Ag device was 0.56, also indicating a diffusion-like behavior. Note that besides the SHG peak motion, a decay of the SHG enhancement was observed at the edge of the source electrode. The decay was very fast for the case of the Au electrode, while it was slow for the Ag. The

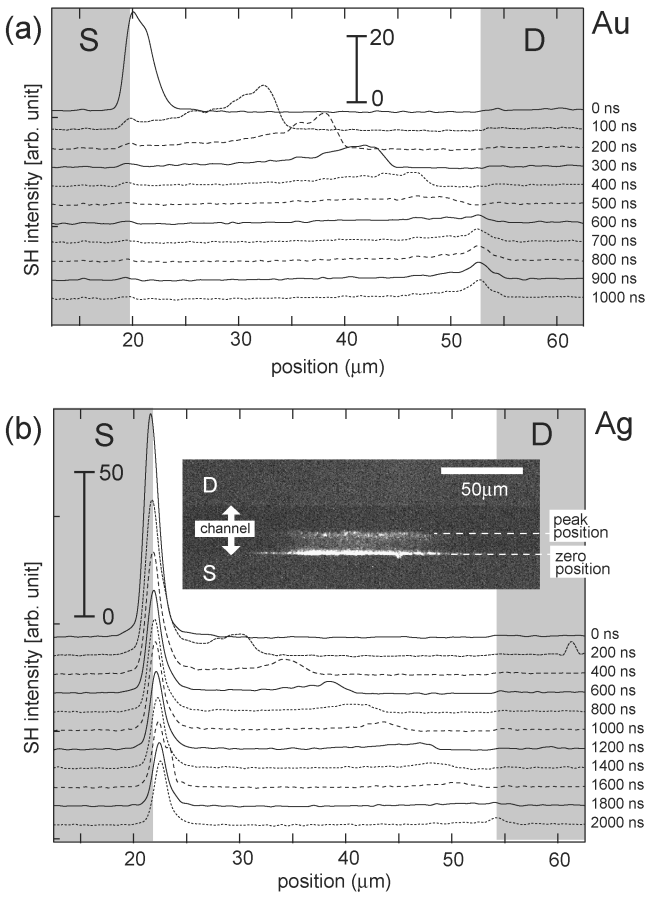

Figure 2. Change in the SHG intensity distribution at different delay times of the pentacene FET using (a) Au and (b) Ag electrodes. Gray-colored regions indicate the electrodes. The inset in b is an actual SHG image from the OFET channel after applying the pulse of 100 V.

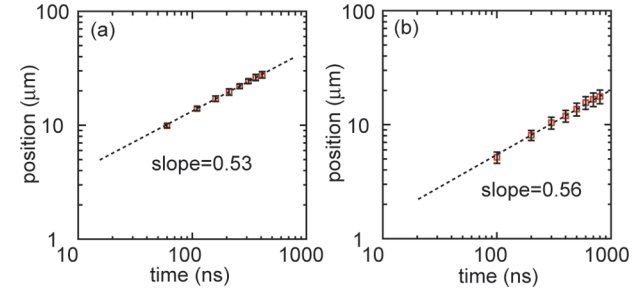

Figure 3. log−log scaled time evolution of the peak position of the SHG intensity in the cases of (a) Au and (b) Ag electrodes after applying the pulse of 100 V. The error bars indicate a standard deviation. The lines are the corresponding fittings, and their slopes are indicated.

intriguing behavior was also observed at various experimental conditions, e.g., low and high temperatures (data not shown).

IV. Discussion

A. Carrier Injection and Transport. Positive voltage applied to the Au source electrode injects holes easily into the pentacene because of the low barrier height between the metal and pentacene for the hole injection. The fact that the SHG intensity at the electrode edge immediately disappeared (less than 100 ns) after the voltage application indicates a rapid decay of the electric field around the source electrode. It is reasonable to argue that the carriers are adequately accumulated at the pentacene/SiO_2 interface under the source electrode and in the channel to compensate the external electric field due to the source potential. This also implies that the channel potential under the source electrode is approximately equivalent to the source potential for the Au electrode. As presented in our previous paper,[14] the SHG intensity at the electrode edge under the negative pulse application scarcely changed with different delay times within the present time scale. This indicates the difficulty of electron injection from the Au electrode because of a high injection barrier formed between the lowest unoccupied molecular orbital (LUMO) of pentacene and the Fermi level of Au. In other words, the SHG intensity at the electrode edge reflects the potential generated across the pentacene below the source electrode. Interestingly, enhancement of the SHG signal was observed around the drain electrode with an increase of delay times (delay time > 600 ns), which indicates a space charge field induced by the holes involving carrier transport makes a significant contribution.

By contrast, for the device with the Ag electrode, the SHG intensity at the electrode edge gradually decreased and seemed to be saturated at 2000 ns, as shown in Figure 2b. Hence, the SHG signal from the electrode edge remained even after reaching a steady state (SS). In other words, even in a steady state the electric field remains at the electrode edge after a positive voltage is applied. This implies that the accumulation of the injected charges in the device is insufficient; i.e., a built potential by the induced charges is small, and the electric field at the edge of electrode is not fully canceled out. Further, the enhancement of the SHG signal was scarcely observed around the drain electrode, which indicates a space charge field caused by the accumulated holes is small. This observation stimulated us to compare the charge carrier injection barriers between Au and Ag electrodes. The work functions of Au and Ag are 5.1 and 4.3 eV, respectively.[16] Given a pentacene with an energy gap of 2.5 eV and an ionization potential of 2.6 eV,[17] the injection barriers for holes are 0.0 and 0.8 eV, correspondingly.

For a better understanding of the experimental observations, we modeled and calculated the transient distributions of the carrier and electric field in the pentacene FET, based on the self-consistent solving of two-dimensional (2D) coupled diffusion-drift and the Poisson equations.[18] For the numerical calculations, the field-independent mobility was assumed to be 0.01 $cm^2/(V\ s)$, and the relative dielectric constant of the pentacene is 3. Other relevant simulation parameters have been shown in Figure 1c. Only hole carriers are presented in the current simulation because the pentacene is p-type, which was also confirmed by the previous experimental observation.[14] We modeled the electrode contact as thermionic emission controlled[17,19] with injection barriers of 0.2 and 0.5 eV and treated the pentacene as a dielectric layer. They are respectively close to the "standard" injection barriers of Au and Ag metioned above. The hole carriers cannot penetrate through the boundary between the pentacene layer and gate insulator (SiO_2). In our simulation the ratio of the channel length and the thickness of the pentacene and gate insulator was chosen as 5 μm/100 nm, which was close to the actual device geometry with pentacene and the gate insulator comprised of SiO_2 (500 nm) and PMMA (100 nm), 30 μm/700 nm. The difference between the geometrical sizes used in the simulation and experiment is not significant, because the magnitude of the electric field E_x in the simulated device was comparable with that in the actual experimental size: about 1.0 and 2.3 V/μm along the channel direction of the FET in the simulation and experiment, respectively.

Figure 4 shows the simulated transient distributions of the carriers, electric field, and potential in the OFET at different times after switching the gate and drain voltages to −5 V at t

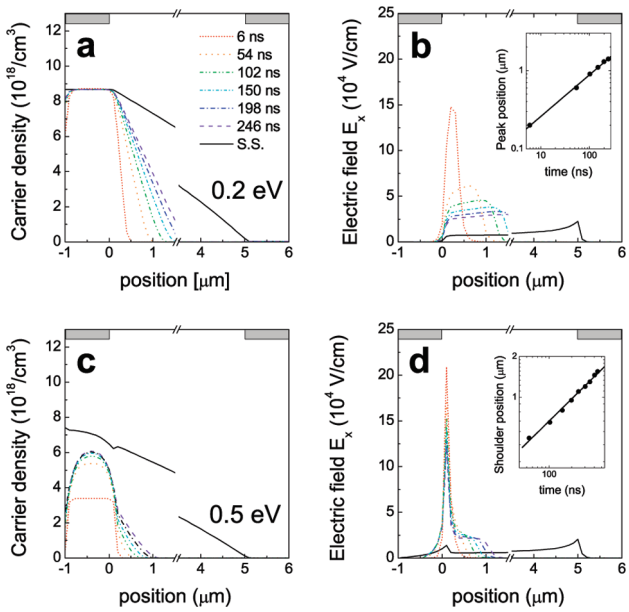

Figure 4. Simulated transient profiles of the carrier density and electric field E_x along the channel at the insulator and pentacene film interface. The hole injection energy barriers of a and b are 0.2 eV, and those of c and d are 0.5 eV, respectively, and applied voltage of −5 V. We also show the profiles in steady state. The gray bars at the top of the panels represent the regions of the source and drain electrodes. Insets illustrate the time evolutions of the peak and shoulder position for the 0.2 and 0.5 eV cases in log−log scale, respectively.

= 0. Here we are only concerned about the distributions at the insulator/organic interface because the carriers are confined near the interface. Several important features were revealed in the simulation. First, for the lower barrier case the carrier density under the electrode is almost constant and invariable with time (>1 ns) after switching the gate voltage. In contrast, for the higher barrier case the density evolves into a parabolic form and is increasing slowly. Second, the shapes of the potentials are almost consistent with the shapes of the densities, which well-supports our simple conjecture that the electric field distribution reflects the carrier distribution in the OFET. Particularly, for the lower barrier case the potential under the source was very close to the source voltage (0 V here); i.e., a potential drop was almost negligible. Finally, the migration way of the electric field depends on the injection barrier that is the only adjustable parameter in the simulation. Because the profile of the SHG intensity well-reflects the profile of the electric field, the migration behaviors revealed by the simulation reproduced those observed in the experiment. Intriguingly, in both cases the migration of the peak or shoulder follows a pattern of the square root of time, as shown in the insets of Figure 4: both of them have an identical slope of 0.54 in the log−log scale.

One of important results disclosed by the simulation is that, the distinct transient electric field and carrier distributions induced by the different electrode metals are the consequence of the distinct barrier height for the hole injection. Because of the 2D characteristic of the OFET, the lower carrier density induces a stronger injection current from the edge of the source (the edge current below) by enhancing the local image potential. This vertical current compensates the loss of the carriers due to drift. If the compensation rate is comparable with the velocity of the drift, the carrier density under the source edge holds fixed; otherwise the density will decay with time. According to the thermal emission mechanism, the edge current for the lower barrier case is far larger than the current for the higher barrier

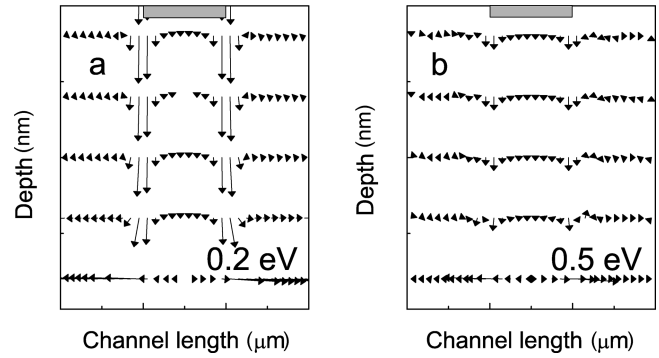

Figure 5. Simulated vector field of the current density under the source at 246 ns. The hole injection energy barriers are (a) 0.2 and (b) 0.5 eV, respectively, and applied voltage of −5 V. The length of the vectors represents the relative strength of the current density. The gray bars at the top of the panels represent the regions of the source electrodes. We show only a small region (10 nm) above the insulator/organic interface.

case. To support these pictures, we showed the simulated vector field of the current density under the source electrode at 246 ns in Figure 5. Therefore, in the case of the injection barrier of 0.2 eV we saw that the carrier density under the source maintains a constant, while in the case of 0.5 eV the density under the source edge becomes parabolic while time increases (Figure 4a,c). Carriers injected from the source electrode are excess charges in the device, and they are acting as the source of the space charge electric field in the OFET. Hence, at the source electrode the local electric field is created by the applied field as well as the space-charge field of injected carriers, which is compensating for the applied field. Hence, the potential difference in pentacene films decay in proportion to the amount of excess charges in OFET. This situation is similar to a case of space charge limited current (SCLC) flowing across insulating film sandwiched between metal electrodes, where carriers decrease the local electric field at the injection electrode to zero in the steady state.[20] In other words, the electric field at the injection electrode is relaxed by the potential built in films by injected carriers. This analysis would be also true for the real cases.

While for the square root of time dependence of the peak/shoulder position, in the following we presented a quantitative analysis inspired by the simulation. Considering that carrier dynamics determines the transient electric field in the OFET, we first approximated the carrier density $p(x,t)$ at the interface as

$$p(x,t) \simeq h(t)[1 - x/(\alpha t^{\gamma})] \quad (1)$$

where αt^{γ} with constants α and γ represents a distance that is an extrapolation of the linear part of the carrier density and where the density becomes zero, and the time-dependent carrier density below the source electrode $h(t) = h_0(1 - \exp(-t/\tau))$ corresponds to the injection and accumulation processes with a relaxation time τ. The linear form of the density was easily understood from Figure 4. The choice of an exponential decay for the carrier density at $x = 0$ was due to the following reason: the carrier density reflects the carrier accumulation process under the source electrode, and this process is generally ruled by the Maxwell−Wagner effect[21] and described in a form of exponential function with relaxation time τ determined by the system.[22] Apparently, eq 1 is valid only for x between 0 and αt^{γ} and the time after the establishment of a linear density.

Substituting eq 1 into the drift-diffusion equation at the interface, $\partial_t p(x,t) = -\partial_x[\mu E_x(x)p(x,t)] + D\,\partial_x^2 p(x,t)$ with the hole mobility μ and diffusion coefficient D, we obtained the following relation,

$$\mu \simeq \frac{\delta}{|V_{gs}|}\frac{\bar{x}^2}{t} \quad (2)$$

where the parameter δ reaches values γ and $(1 - \gamma)$ for the low and high injection barriers, respectively. Importantly, this equation provides a way to evaluate the mobility on the basis of the TRM-SHG measurement for the different devices using the Au and Ag electrodes. Using TRM-SHG data shown in Figure 2, mobilities were evaluated to be 0.11 and 0.06 $cm^2/(V\,s)$ for Au and Ag electrodes, respectively. To evaluate the mobility using the Ag electrode, a potential drop was explicitly taken into account. Here, the potential drop represents the potential difference between the source electrode and the channel below the source electrode. Accordingly, the potential drop was estimated to be approximately 8.4 V for the present case. Interestingly, the evaluated mobility of the device using the Au electrode reached almost the identical value as that using the Ag electrode if the measurement was performed under an application voltage of 60 V.[23] This clearly indicates that the transport properties are identical between the two different devices using the Au and Ag electrodes.

Here we must point out several results of eq 2. First of all, the peak position of the electric field (or the SHG intensity in the experiment) is propagating in terms of the square root of time. It is interesting to note that the square-root dependence is not influenced by the real value of the power exponent γ. Although comparison of evaluated mobility from the simulation result of low and high injection barrier by eq 2 leads to $\gamma = 0.7$ and 0.1, reflecting the difference in the interaction between carriers, respectively, the square root of time dependence was conserved in the simulation as well as in the experimental results (see Figure 3a,b]. On the other hand, eq 2 could be derived in simplified form from the group velocity of the carriers $\partial_t \bar{x} = \mu|V_{gs}|(t)/\bar{x}$ as follows: $\mu = \tau\bar{x}^2/(|V_{gs}|t^2)$. Here we used a short-time approximation $V_{gs}(t) \simeq V_{gs}t/\tau$. This result is identical to eq 2 for short times and $\gamma \ll 1$.

B. Channel Charging. As discussed previously, the negligible potential drop was observed at the pentacene−Au contact, indicating the carriers were adequately accumulated under the source electrode, and they were contributing to build a potential that canceled the electric field formed by the applied voltage to the source electrode. The accumulated charge density at the pentacene/insulator interface is comparable to the charge accumulated by the SiO_2 gate capacitor, which is given by $C_{gs}V_{gs}$. This value was evaluated as 3.45×10^{-7} C/cm^2, and it well-accounts for the saturated carrier density under the source electrode in Figure 2a. Here the carrier density at the surface was calculated as 8.5×10^{18} cm^{-3} with a channel thickness of 50 nm, and it could be calculated as 3.52×10^{-7} C/cm^2 after summing up charges in the pentacene under the source electrode. Here the channel thickness of 50 nm was the value used in the simulation. In this way, it is clear that a space charge field formation leads to the decrease of the potential drop under the source electrode. It is interesting to note that the calculated amount of accumulated carriers at the pentacene/insulator interface over the entire region of the channel ($0 < x < 5$ μm) in steady state is about 14% greater than that evaluated on the basis of the Maxwell−Wagner model by taking into account the gradual channel approximation[21] and using the relationship $Q_s^{MW} = C_g(V_{gs} - (1/2)V_{ds})$, where C_g is the gate capacitance. In more detail, the accumulated charge in an insulating film under SCLC flow is generally 12.5% greater than the capacitive charge given by CV, i.e., $(9/8)CV$,[20] where C is the capacitance and V is the applied voltage. Therefore, the difference mentioned above is about 1.5% if we consider the SCLC process for the carrier transport across the OFET. Such agreement is due to the linear-like carrier distribution along the channel, but the finite thickness of the channel may cause the deviation. Further, we should note that the presence of carriers in the FET contributes to the space charge field formation and thus leads to the generation of SHG signal at the drain electrode, as shown in Figure 2a.[24]

On the other hand, the carrier density estimated in the case of the 0.5 eV barrier was quite low, and this indicates the insufficient accumulation under the source electrode, followed by decreases of the charge carrier density along the channel. Interestingly, the linear-like dependence is conserved in steady state. Thus, by applying a similar approach, we obtained identical correspondence of results except that a potential under the source electrode accompanies the potential drop. This comparison shows the accuracy of the present approach also for metals with various injection barriers if the potential drop is included. Finally, we should note that this approach will be also valid if the potential drop is caused by complicated interfacial energetics.

V. Conclusion

The TRM-SHG method was used to investigate the transport and injection behaviors of the carriers in the pentacene FET by directly observing the migration of the electric field in the devices. For the device with Ag electrode, insufficient accumulation of the carriers at the channel leading to the potential drop was observed, whereas the carriers accumulate sufficiently for the device with the Au electrode. The difference in the electric field migration is presumably due to the distinct barriers for the carrier injection. Nevertheless, numerical simulation based on 2D coupled diffusion-drift and the Poisson equation well-supported the experimental results. Although the behavior was quite different between Ag and Au electrodes, we proposed a simple general model suitable for the mobility estimation. Evaluated carrier mobility in the FET channel was independent of the metal electrode, indicating that transport properties were identical between the devices using Au and Ag electrodes. These results clearly indicate that the TRM-SHG technique is useful in studying the carrier dynamics in the OFET.

Acknowledgment. This work was supported by the Grants-in-Aid for Scientific Research (Grant Nos.18686029 and 19206034). Support from the New Energy and Industrial Technology Development Organization (NEDO) are also gratefully acknowledged. F.L. thanks the Tokyo Institute of Technology, where this work was completed, for its hospitality.

References and Notes

(1) Yasuda, T.; Goto, T.; Fujita, K.; Tsutsui, T. *Appl. Phys. Lett.* **2004**, *85*, 2098.

(2) Chua, L. L.; Zaumseil, J.; Chang, J. F.; Ou, E. C. W.; Ho, P. K. H.; Sirringhaus, H.; Friend, R. H. *Nature* **2005**, *434*, 194.

(3) Zaumseil, J.; Friend, R. H.; Sirringhaus, H. *Nat. Mater.* **2006**, *5*, 69.

(4) Sze S. M. *Physics of semiconducting devices*, 2nd ed.; Wiley: New York, 1981.

(5) Knipp, D.; Street, R. A.; Volkel, A. R. *Appl. Phys. Lett.* **2003**, *82*, 3907.

(6) Guo, D.; Ikeda, S.; Saiki, K.; Miyazoe, H.; Terashima, K. *J. Appl. Phys.* **2006**, *99*, 094502.

(7) Ishii, H.; Sugiyama, K.; Ito, E.; Seki, K. *Adv. Mater.* **1999**, *11*, 605.

(8) Chu, C.-W.; Li, S.-H.; Chen, C.-W.; Shrotriya, V.; Yang, Y. *Appl. Phys. Lett.* **2005**, *87*, 193508.

(9) Waldauf, C.; Schilinsky, P.; Perisutti, M.; Hauch, J.; Brabec, C. J. *Adv. Mater.* **2003**, *15*, 2084.

(10) Zheng, Y.; Qi, D.; Chandrasekhar, N.; Gao, X.; Troadec, C.; Wee, A. T. S. *Langmuir* **2007**, *23*, 8336.

(11) Cheng, H. L.; Chou, W. Y.; Kuo, C. W.; Tang, F. C.; Wang, Y. W. *Appl. Phys. Lett.* **2006**, *88*, 161918.

(12) Koyanagi, T.; Furukawa, S.; Tsutsui, K.; Wada, Y.; Furukawa, Y. *Vib. Spectrosc.* **2006**, *42*, 156.

(13) Ye, H.; Huang, J.; Park, J.-R.; Katz, H. E.; Gracias, D. H. *J. Phys. Chem. C* **2007**, *111*, 13250.

(14) Manaka, T.; Lim, E.; Tamura, R.; Iwamoto, M. *Nat. Photonics* **2007**, *1*, 581.

(15) Manaka, T.; Liu, F.; Weis, M.; Iwamoto, M *Phys. Rev. B* **2008**, *78*, 121302.

(16) Michaelson, H. B. *IBM. J. Res. Dev.* **1978**, *22*, 72.

(17) Davids, P. S.; Campbell, I. H.; Smith, D. L. *J. Appl. Phys.* **1997**, *82*, 6319.

(18) Snowden, C. M. *Semiconductor device modelling*; Peter Peregrinus: London, 1988.

(19) Tessler, N.; Roichman, Y. *Appl. Phys. Lett.* **2001**, *79*, 2987.

(20) Lampert, M. A.; Mark, P. *Current injection in solid*; Academic Press: New York, 1970.

(21) Tamura, R.; Lim, E.; Manaka, T.; Iwamoto, M. *J. Appl. Phys.* **2006**, *100*, 114515.

(22) Manaka, T.; Lim, E.; Tamura, R.; Iwamoto, M. *Jpn. J. Appl. Phys.* **2008**, *47*, 1301.

(23) For the device using Ag electrode, effective voltage applied to the pentacene layer is expressed as $C_g/(C_g + C_{pen})V_{gs} - V_{drop} = 12.7$ V at $V_{gs} = 100$ V. To apply the same voltage to the pentacene layer of Au device without a potential drop, we chose $V_{gs} = 60$ V, because $12.7(C_g + C_{pen})/C_g = 60$ V.

(24) Yamada, D.; Manaka, T.; Lim, E.; Tamura, R.; Weis, M.; Iwamoto, M. *J. Appl. Phys.* **2008**, *104*, 074502.

JP900779D